Tuberculosis 118 (2019) 101855

Contents lists available at ScienceDirect

Tuberculosis

journal homepage: www.elsevier.com/locate/tube

Mechanisms of Pathogenesis

Mycobacterium bovis sigF mutant exhibits altered surface phenotype and compromised pathogenesis

Debashis Dutta[a,b,1], Vishal Srivastava[b,1], Ashutosh Tripathi[b], Vandana Singh[b], Mohd Mustkim Ansari[b], Garima Pant[c], Manisha Mishra[d], Sharad Sharma[e], Jagadehswar Reddy Thota[f], Pradhyumna Kumar Singh[d], Bhupendra N. Singh[b,*]

[a] Department of Immunology and Microbiology, The Scripps Research Institute, 130 Scripps Way, 3C1, FL33458, USA
[b] Division of Microbiology, CSIR-Central Drug Research Institute, Lucknow, 226031, India
[c] Electron Microscopy Unit, CSIR-Central Drug Research Institute, Lucknow, 226031, India
[d] CSIR-National Botanical Research Institute, Lucknow, 226001, India
[e] Division of Toxicology and Experimental Medicine, CSIR-Central Drug Research Institute, Lucknow, 226031, India
[f] Sophisticated Analytical Instrument Facility, CSIR-Central Drug Research Institute, Lucknow, 226031, India

1. Introduction

Mycobacterium bovis belongs to the *Mycobacterium tuberculosis* complex (MTBC) which displays the broadest spectrum of host infection affecting humans, bovines and goats [1]. They succeeded as a pathogen due to its ability to adapt to a range of stresses imposed by the host immune system. They sense the host cellular environment and regulate their gene expression in response to prevailing conditions. Gene expression in bacteria is regulated primarily at the level of transcription initiation. Sigma factors guide the RNA polymerase enzyme complex to specific promoter sequences to initiate transcription of genes. *M. bovis* genome encodes 13 sigma factors [2]. The sigma factor F, SigF, was deemed as a stationary phase stress response sigma factor present only in slow-growing mycobacterial species [3]. However, later it was found to be widely conserved among mycobacteria [4,5]. In mice, the *M. tuberculosis* Δ*sigF* mutant showed attenuated disease pathology [6,7]. In non-tuberculous, rapid-growing mycobacteria, *sigF* is constitutively expressed throughout the growth, suggesting its wider role in mycobacteria in addition to virulence gene regulation in *M. tuberculosis* [5,8]. In *M. tuberculosis* SigF regulon largely comprises genes with predicted roles in stress response and virulence [9,10]. In *M. smegmatis* SigF regulon identified genes reportedly involved in oxidative stress and stationary phase adaptation [11,12].

In this study, we report a detailed analysis of the surface phenotype of the Δ*sigF* mutant in *M. bovis*, its proteome profile and *in vivo* pathogenicity in a mouse model. The mutant displayed distinct colony morphotypes suggestive of altered surface properties, which were largely restored in the complemented Δ*sigF* mutant. Comparative proteomics and lipid analysis of the mutant and wild type strains provided a rationale for the mutant's *in vitro* and *in vivo* phenotypes. Proteome analysis of *M. bovis* biofilms highlighted the role of SigF regulated proteins in biofilm formation as they appeared down-regulated in the Δ*sigF* mutant. The degree of pathogenesis in a mouse model was assessed by time-to-death and bacterial burden analysis.

2. Materials and methods

Ethics statement. BALB/c mice were obtained from the animal house facilities of Central Drug Research Institute (CDRI), Lucknow, India. The protocols used in this study were reviewed and approved by the Institutional Animal Ethics Committee (IAEC) (Approval No. IAEC/2013/41). Experiments were performed using the biosafety facility of the institute.

Bacterial strains, plasmids and cultures. Bacterial strains and plasmids used in this study are described in Table 1. *E. coli* cultures were grown in Luria-Bertani (LB) broth with addition of ampicillin (100 μg/ml), kanamycin (25 μg/ml) and hygromycin (100 μg/ml), as required. *M. bovis* and derivative strains were grown at 37 °C in Middlebrook 7H9 (Difco) liquid culture medium supplemented with 10% albumin-dextrose-catalase (ADC), 0.2% glycerol and 0.025% Tween-80 or on Middlebrook 7H11 (Difco) solid culture medium supplemented with 10% oleic acid-albumin-dextrose-catalase (OADC) (BD Biosciences) and 0.5% glycerol.

DNA manipulations, construction of *sigF* mutant and its complementation. Recombinant DNA techniques were performed as per standard procedures [13]. Restriction and modifying enzymes were

* Corresponding author.
E-mail addresses: ddutta@scripps.edu (D. Dutta), genius.vishu@gmail.com (V. Srivastava), 1ashutripathi@gmail.com (A. Tripathi), singh.vandana02@gmail.com (V. Singh), mustkim.bhu@gmail.com (M.M. Ansari), garimajune2@gmail.com (G. Pant), manisha.nbri@gmail.com (M. Mishra), sharadmandira@yahoo.com (S. Sharma), tjreddy@cdri.res.in (J.R. Thota), pksingh@nbri.res.in (P.K. Singh), bnsingh@cdri.res.in (B.N. Singh).
[1] these authors contributed equally to this paper.

https://doi.org/10.1016/j.tube.2019.07.006
Received 2 November 2018; Received in revised form 26 July 2019; Accepted 29 July 2019
Available online 31 July 2019
1472-9792/

Table 1
Strains, plasmids and primers used in this study.

Strains and plasmids	Relevant details	Source
Strains		
NEB10	*galU recA1 endA1 G rpsL* (StrR)*Δ(mrr-hsdRMS-mcrBC)*	New England Biolabs
DH5α	*rec*A1 *end*A1 *hsd*R17 (rK–, mK +) *pho*A *sup*E44 λ– *thi*-1	Invitrogen
M. bovis (AN5)	Wild type *M. bovis* used in this study.	JALMA, India
Mb10	*M. bovis* Δ*sigF* mutant, hyg^r	This study
Mb11	Mb10 complemented with *M. bovis* $sigF^+$ allele, km^r, hyg^r	This study
Mb10/MS	Mb10 Δ*sigF* mutant complemented with *M. bovis* malate synthase gene along with $hsp60_{pr}$ (merodiploid stain km^r, hyg^r)	This study
Plasmids		
pTZ57 R/T	TA cloning vector, amp^r	Fermentas
pDrive	TA cloning vector, amp^r, km^r	Qiazen
pDSFKO5	5' flanking sequence cloned in pDrive, amp^r, km^r	This study
pTZSFKO3	3′ flanking sequence cloned in pTZ57R/T. amp^r	This study
pDBSFKO	5′ and 3′ flanking sequences in pDrive, amp^r, km^r	This study
pDBSFKOH	hyg^r introduced between 5' and 3' sequence in pDrive, hyg^r, km^r	This study
pPR27	Allelic exchange vector gm^r, gift from late Jean Marc Reyrat	
pPRBSFOH	5′,3' with hyg^r cloned in pPR27at XbaI and BamHI, gm^r, hyg^r	This study
pTZFr2	Clone of 5′ flank to confirm HR, amp^r	This study
pTZFr3	Clone of 3′ flank to confirm HR, amp^r	
pTZMb4	Complementation cassette in pTZ57 R/T, amp^r	This study
pTVR	Derivative of pMV261, km^r	Lab stock
pTVRMb4	Complementation cassette in pTVR, km^r	This study
pMV306	Integrative vector km^r, kind gift from W. R. Jacobs Jr.	
pMV306MS28	Complementation cassette in pMV306, km^r	This study

Primers (*sigF* and 5'-, 3'-flanks)	
MbSFKO1	GCATGCCGACCACTTGCGGACGACG
MbSFKO2	ACTAGTCAAGCACCGCTGAACGATC
MbSFKO3	ACTAGTTCTCACAGATGCACGTGTC
MbSFKO4	GCATGCCGGCCTGCCGATCGCGATC
SF1	TCCATATGACGGCGCGCGCT
SF3	CACAAGCTTGGCTACTCCAACT
For allelic exchange validation	
KO3R2	CGACCTGGGCGACAAGGTCA
HKO1	CTTCGCCCTCCGAGAGCTGCA
HKO2	CTGGACCGATGGCTGTGTAGA
KO5F3	GTTGATCCGCCAGCTGTGGCA
HygF	ATGAAAAGCCTGAACTCAC
HygR	GTTTCAGGCAGGTCTTGCA
HygP2	ACGTTCTGGACGGACTTTG
For complementation	
MbSFC1	GCTGGGATCCTAGACATCCTAGT
MbSFC2	GAGTTGTCGACGCACCCTCCCGG
MbSFC3	GTGCGTCGACTGACTCGGATTT
MbSFC4	AGCCTCTAGACTACTCCAACTGA
For Real time RT-PCR	
SigART1 (*sigA*)	GTGGCAGCGACCAAAGCAAG
SigART4	CACTAGCGGACTTCGCCGCT
Mb1868cRTF (*glcB*)	CGGGTGCTCTACGACTTCGT
Mb1868cRTR	GCGGGCGTTCAACAGAGCTT
Mb1123RTF (*glyA1*)	CTGAGGTTGACCCCGATATC
Mb1123RTR	GTTGGTCAGCACACTGCCCT
Mb1051RTF (*eno*)	AGAGATCCTCGATTCCCGCG
Mb1051RTR	GTTGGTCAGCACACTGCCCT
Mb2169cRTF (*wag31*)	CGTCCACAATGTGGCGTTCA
Mb2169cRTR	CTCTGACGCAGATCGGAGTT
Mb0655RTF (*hadB*)	TGAAGGTCGGAGACCAGCTT
Mb0655RTR	ATCTCGTCGTCCCAGTGAAT
Mb1128cRTF (*fum*)	CCAATTACCGCATCGAGCAC
Mb1128cRTR	CGGCCGGATATCGGGAAGTT
For heterologous expression	
Mb1868cF (*glcB*)	CTATCTAGATGACAGATCGCGTGTGGT
Mb1868cR	TCATGAATTCCTAGCGGGCCGCATCGTC

amp^r-ampicillin resistant, $hygro^r$-hygromycin resistant, km^r-kanamycin resistant, gm^r - gentamycin resistant, HR - homologous recombination.

procured from Fermentas, India. Primers used in this study are listed in Table 1. *M. bovis sigF* deletion mutant was generated using allele exchange method and validated by PCR, sequencing and Southern hybridizations (for details see supplementary data). Southern hybridization was performed using Dig-labeled probes that were PCR amplified using specific primers (Fig. 1). One of the *sigF* deletion mutants, Mb10, was chosen for further studies. Mb10 was complemented with an integrative plasmid vector pMV306 containing *M. bovis sigF* along with *rsbW* (anti-sigF) coding sequences and the upstream native *sigF* promoter. The *rsbW* and *sigF* coexist and are cotranscribed in mycobacteria (Fig. 1A). To ensure that only native RsbW remains functional and a stoichiometric balance between RsbW and SigF is maintained, *rsbW* ORF in complementing cassette was made non-functional by mutating its start codon. This ensured that the complemented strain gets the

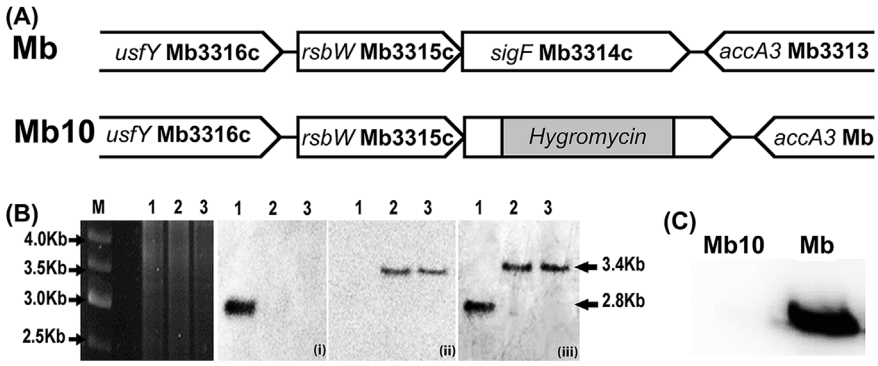

Fig. 1. Southern based confirmation of *M. bovis* Δ*sigF* mutant (Mb10). (A) *sigF* locus map in *M. bovis* wild type (Mb) and Δ*sigF* mutant (Mb10). In Mb10, hygromycin-resistance gene is flanked by a part of *sigF* on either side. (B) BamHI-restricted genomic DNAs from different *M. bovis* strains (Lanes: 1- wild type (Mb), 2- Δ*sigF* mutant-1 (Mb10), 3- Δ*sigF* mutant-2) were hybridized using specific probes: internal *sigF* deleted region (probe − 1), hyg region (probe − 2) and region adjacent to *sigF* deleted sequence (probe-3) to blot (i), (ii) and (iii), respectively. The DNA Ladder (M) and hybridizing bands are indicated at left and right margin, respectively. For details see Fig. S1, supplemental data. (C) Western blot showing absence of the SigF in Mb10. Immunodetection using SigF antibody was described earlier (12).

RsbW functional copy only from its native locus. The complemented strain was designated as Mb11. To generate a merodiploid strain (Mb10/MS), the Δ*sigF* mutant (Mb10) was transformed with the *M. bovis* malate synthase (MS) gene (Mb1868c) under transcriptional control of *hsp60* promoter in a pMV261 plasmid vector.

Pellicles and biofilms formation and their analyses. *M. bovis* biofilms were developed in 12-well polystyrene plates as described earlier [14]. For pellicles formation, cultures were allowed to grow in glass vials without shaking. Pellicles appeared at the interface of air and medium inside the vials (Fig. 6A). For biofilms, *M. bovis* culture grown in Middlebrook 7H9 medium (1.0 OD_{600}) were diluted 1:100 in Sauton's medium without detergent and added to each well. The wells were covered with parafilm and incubated at 37 °C for 5 weeks without shaking. The isolates of *M. bovis*, Mb10 and Mb11 strains were then assessed visually for their ability to form biofilms. For quantitative assessment of biofilms crystal violet assay was performed as described previously [15]. The medium underneath the biofilm was carefully removed from wells, biofilms were dried in biosafety cabinet and incubated with 500 µl of 1% crystal violet for 10 min. Wells were washed three times with water and dried again. 1 ml of 95% ethanol was added to each well, incubated for 10 min and the absorbance was determined after 3-fold serial dilutions at 570 nm on a spectrophotometer (BioRad). For DNase treatment, fully formed *M. bovis* biofilms in polystyrene plate's wells were treated with phosphate buffer saline (PBS), PBS with reaction buffer, PBS with 10 units DNase I (Ambion), reaction buffer with heat inactivated DNase I and reaction buffer with DNase I for 3 h at 37 °C. Following this, biofilms were quantified by crystal violet staining as described above. Selected *M. bovis* strains were repeatedly analysed in at least three independent biological assays.

Scanning Electron Microscopy (SEM). *M. bovis* wild type, Mb10 mutant and Mb11 complemented strain cultures were grown in MB7H9 broth. Full grown cultures (2.0 OD_{600}) were centrifuged at 400 × *g* for 5 min and fixed with 2.5% glutaraldehyde in 0.1 M phosphate buffer (pH 7.4) for 3 h at room temperature followed by osmication and dehydration in ascending series of ethanol. Samples were critical point dried using a Baltec CPD followed by mounting them on specimen holders (stubs) and sputter coating with Au-Pd alloy. Samples were then analyzed under a FEI Quanta 250 Scanning Electron Microscope. The imaging conditions are mentioned in the data bar of the SEM micrographs.

Extraction and analysis of lipids. Extractions and analysis of lipids were performed as described in previous studies [12]. Lipids were extracted from equal mass of freeze dried stationary phase grown *M. bovis* wild type, Mb10 and Mb11 cultures (see supplementary data). Polar and nonpolar lipids were separated by 2D-TLC and developed using different solvent systems: **System A:** (1) petroleum ether/ethyl acetate (98:2, run three times in first dimension) (2) petroleum ether/acetone (98:2, run once in second dimension). **System D:** (1) chloroform/methanol/water (100:14:0.8, run once in first dimension) (2) chloroform/acetone/methanol/water (50:60:2.5:3, run once in second dimension). Identification of lipid spots was carried out by comparing scanned images with previous published results [16].

Nile red and EtBr uptake assay. Accumulation of Nile Red (Sigma) and ethidium bromide (EtBr) (OmniPur) was measured as described earlier [16]. Briefly, *M. bovis* wild type, Δ*sigF* mutant (Mb10) and complemented strain (Mb11) culture (0.8–1.0 OD_{600}) were washed with 50 mM potassium phosphate buffer (pH 7.0) and then resuspended in 2 ml of the same buffer. The OD_{600} of the resuspended cells was adjusted to 0.4 and 100 µl of this cell suspension was added in triplicate to a 96-well black fluoroplate. Nile Red and EtBr were added to final concentrations of 2 µM and 6 µM, respectively. The accumulation of dyes was measured by fluorescence using a spectrofluorometer with an excitation of 544 nm and emission of 630 nm for Nile Red and an excitation of 545 nm and emission of 600 nm for EtBr. All experiments were performed in triplicate and repeated at least twice, yielding similar results.

2D-Gel electrophoresis and mass spectrometry. Total cellular proteins were prepared from stationary phase cultures of *M. bovis* wild type and Δ*sigF* mutant grown in MB7H9 medium. For biofilms and planktonic cultures, *M. bovis* wild type strain was grown to 0.8 OD_{600} without Tween-80. Then cultures were split into two parts; one was incubated with shaking (180 rpm) while another was incubated without shaking for 30 days to ensure mature biofilm formation. For proteins extraction, biofilms and bacterial cells were washed with phosphate buffer saline (pH 7.0) and resuspended in protein extraction buffer (20 mM Tris-Cl pH 8.0, 25 mM NaCl, 4% 3-[(3-cholamidopropyl) dimethylammonio]-1-propanesulfonate (CHAPS), 2.5% Glycerol, 1% Protease inhibitor cocktail (Roche). Cell suspensions were sonicated (repeated pulses of 20 s on and 20 s off at 25% amplitude for 30 min, centrifuged at 20,000 g for 20 min at 4 °C, and supernatants were collected in fresh tubes. Cell lysates were treated with 15% trichloro acetic acid, incubated overnight at − 20 °C to precipitate proteins that were collected by centrifugation at 13,000 g for 15 min at 4 °C, washed with cold acetone and air dried. The pellets were resuspended in rehydration buffer (7 M urea, 2 M thiourea, 4% CHAPS, 10 mM DTT, 20 mM Tris pH 8.0, 1 mM EDTA). Protein concentration was determined using the Bradford assay. For isoelectric focusing (IEF), immobilized pH gradient (IPG) strips (pH 4-7, 13 cm) (GE Healthcare) were rehydrated overnight at 20 °C with 500 µg protein in rehydration buffer. Strips were focused on Ettan IPG Phor 3 (GE Healthcare) using running program: 100V for 3 h in step mode, 500V for 3 h in gradient mode, 1500V for 3 h in gradient mode and 5000 V in gradient until 45 kVh achieved. The current limit was set at 50 µA per strip. After IEF, IPG strips were equilibrated (15 min) in equilibration buffer (6 M Urea, 75 mM Tris-Cl pH 8.8, 29.3% Glycerol, 2% SDS, 1% Bromophenol blue) containing 130 mM dithiothreitol (DTT) followed by equilibration buffer containing 135 mM iodoacetamide for 15 min. Proteins were then separated in second dimension on 12% SDS-PAGE at 40 mA constant current. Gels were stained with Coomassie Brilliant Blue R250. Images of gels were acquired by Labscan software (GE Healthcare) at 300 dpi in the supported input format MEL (ImageMaster). Gels depicting differential expression of protein spots were analysed using ImageMaster™

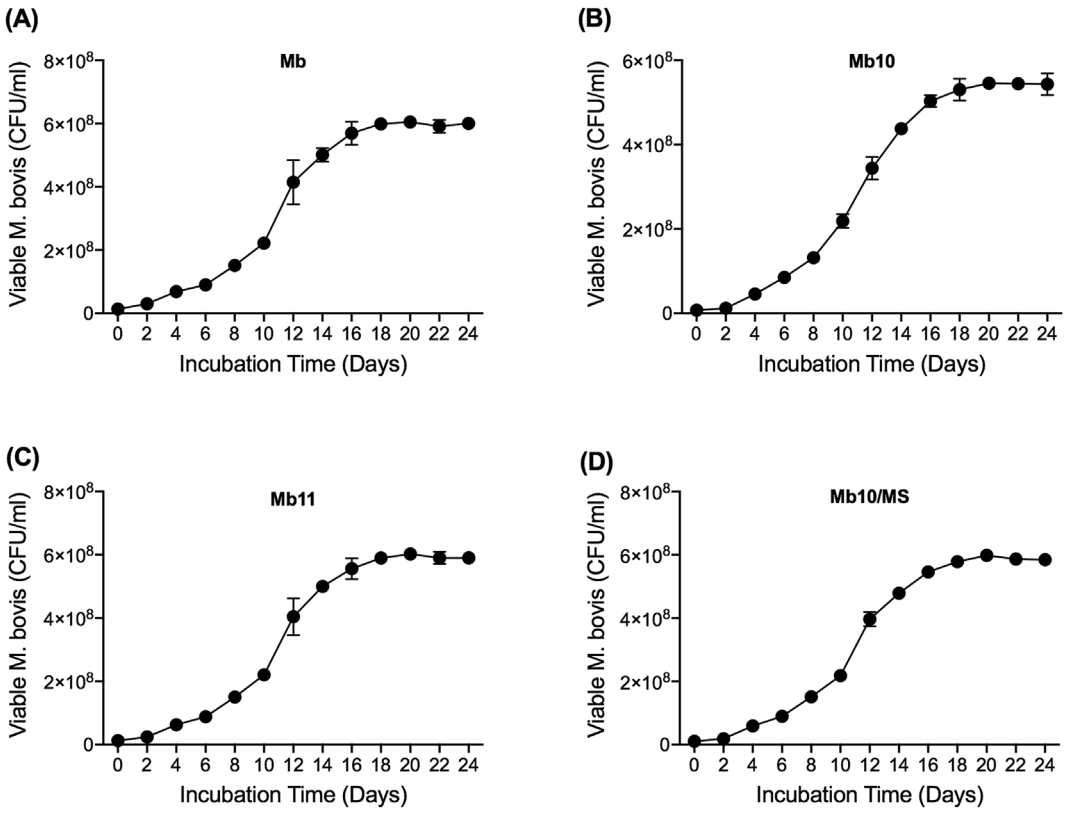

Fig. 2. Growth profile of *M. bovis* wild type (Mb), Δ*sigF* mutant (Mb10), complemented strain (Mb11) and merodiploid strain (Mb10/MS) grown in 7H9 liquid culture medium supplemented with 10% ADC, 0.2% glycerol and 0.025% Tween-80.

2D Platinum 7.0 (GE Healthcare). Software computes the amount of protein present at each spot based on spot intensity, area and volume. Equal amount of proteins were loaded in all gels and experiments were repeated at least three times.

In-gel digestion of differentially expressed protein spot was performed following standard protocol [17]. Details of mass spectrometry are provided in supplementary data. For analysis of MS and MS/MS data, the NCBI database was searched using ProteinPilot software (ABSciex 4.0) and MASCOT. Set search parameters were: taxonomy set to all enteries, trypsin as enzyme (one missed cleavage allowed), fixed precursor ion mass tolerance (20 ppm), fragment ion mass tolerance (0.05 Da), calibration error (0.005 Da), carbamido methylation of cysteines and possible methionine oxidation and peptide charge was set 1^+. Only significant proteins ($p < 0.05$) were filtered. Functional categorization was done using KEGG, Swiss-prot, Bovilist and Tuberculist databases.

RNA extraction and Real-time PCR. RNAs were extracted from *M. bovis* strains using RNeasy kit (Qiagen) according to the manufacturer's protocol. RNA was DNAse treated and DNA-free RNA was reverse transcribed using random hexamers and transcriptor reverse transcriptase (Roche) followed by quantitative Real-Time PCR using SYBR green master II (Roche) as described earlier [18]. Gene specific primers for Real-Time PCR were listed in Table 1. For bacterial mRNA analysis, results were normalized to the amount of *sigA* mRNA. RNA samples that had not been reverse transcribed were included as a control.

Adherence assay. Adherence of *M. bovis* wild type, Mb10 mutant, Mb11 complemented strain and MB10/MS merodiploid strain on the surface of lung epithelial cells (A549) was assessed as described previously [19]. Briefly, log phase bacterial cells were collected by centrifugation (2000g, 5 min), washed three times with PBS and resuspended at 10^6 bacteria per ml. A549 cells (2×10^5 per well) were seeded in each 24 well plate and allowed to form monolayer for 3 days ($4\text{-}5 \times 10^5$ cells). On third day, A549 monolayers were washed three times and 1 ml of bacterial suspension was added to each well in triplicates at moi (10:1) and moi (100:1). Plate was incubated at 37 °C in 5% CO_2, the wells were washed with RPMI-1640 incomplete medium (Sigma) to remove the unbound bacteria. A549 monolayers were lysed by adding 500 µl of 0.1% Triton X-100 per well. Serial dilutions of the lysate were plated on Middlebrook 7H11 plates for colony forming units (CFU) determination. Resuspended bacterial culture, used as inoculum in each well, was also plated separately for CFU determination. The percent adherence was calculated as follows: (no. of CFU recovered from each well/CFU added to each well) × 100.

Virulence studies in mice. Groups of BALB/c mice (44 mice per group) were infected intravenously with mid-log phase cultures (10^6 CFU) of *M. bovis*, Mb10 mutant, and complemented (Mb11) strains. Bacterial implantation in lung was confirmed by sacrificing three animals from each group 24 h post-infection followed by plating of lung homogenate on 7H11 agar plates to determine CFU. To monitor the degree of infection, disease progression and bacterial burden in organs of infected animals, lungs and spleens were removed aseptically at defined time intervals and serially diluted organ homogenates were plated to enumerate CFU (Fig. 11D and E).

Statistical analysis. Statistical analysis of data was performed using GraphPad Prism 7 software. For comparisons between two groups, Students t-test was used. For comparisons between multiple groups, one-way analysis of variance (ANOVA) followed by Tukey's multiple-comparison test was used. Log-rank Mantel-Cox tests were applied to determine the significance of difference in the survival curve. For all analyses, p-value of < 0.05 was considered significant.

3. Results

***M. bovis* Δ*sigF* mutant exhibits altered colony morphology and enhanced cellular permeability.** The *sigF* gene in *M. bovis* was replaced with hygromycin resistance gene and the mutants were

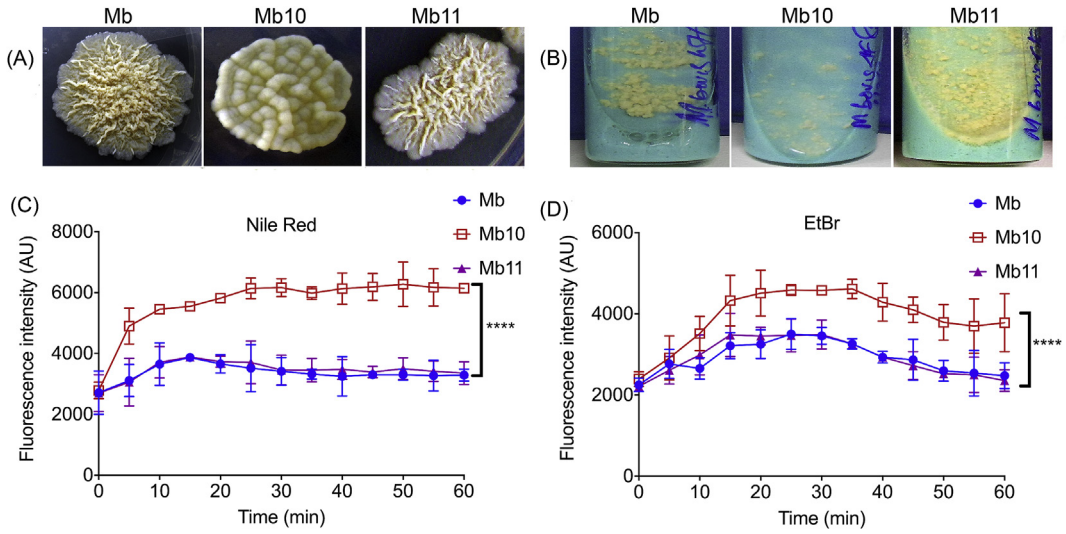

Fig. 3. Colony morphotypes of *M. bovis* wild type (Mb), Δ*sigF* mutant (Mb10), complemented strain (Mb11). (A) Δ*sigF* mutant colonies appear smooth and devoid of cords. (B) Distinct appearance of *M. bovis* strains on LJ slants. Intracellular accumulation of Nile red 2 μM (C) and EtBr 6 μM (D) by *M. bovis* wild type (Mb), Δ*sigF* mutant (Mb10) and complemented strain (Mb11) were measured by fluorescence spectroscopy. The data are means ± SD from three independent experiments (****p < 0.0001). The mutant accumulates more Nile Red and EtBr than the wild type. (For interpretation of the references to colour in this figure legend, the reader is referred to the Web version of this article.)

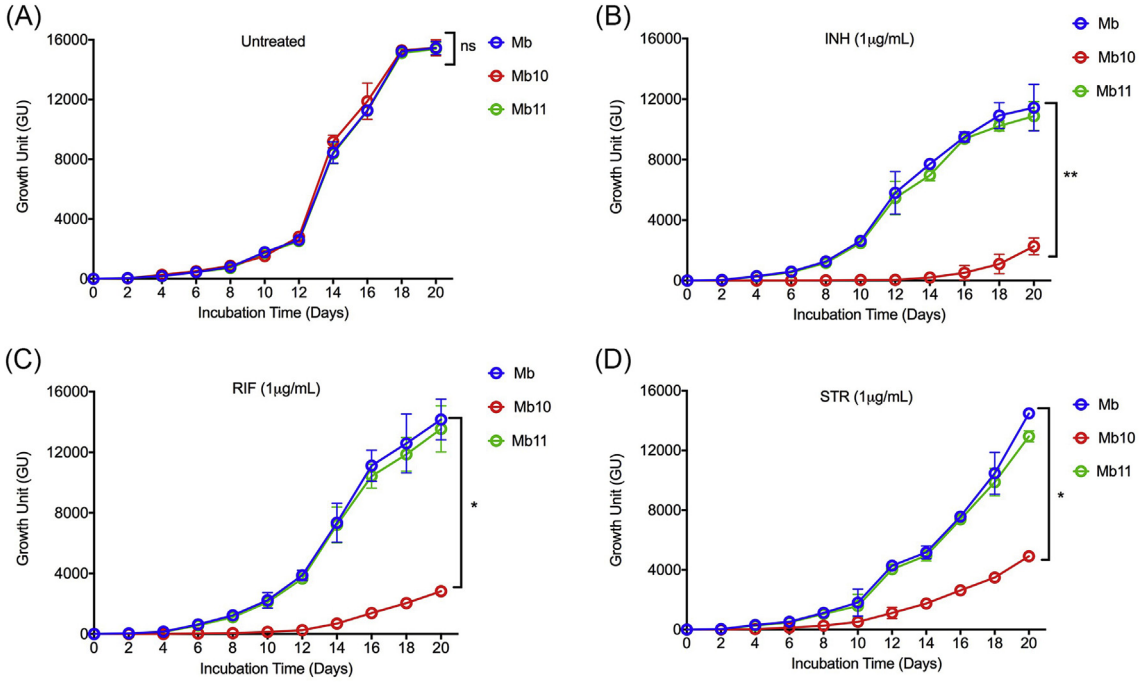

Fig. 4. *M. bovis* wild type (Mb), Δ*sigF* mutant (Mb10) and complemented (Mb11) strains were grown to stationary phase (≥2.0 OD_{600}) and cultures were subjected to different concentrations of drugs for 24 h at 37 °C. Growth and drug susceptibility were analysed using BD MGIT 960 BACTEC system. Experiments were set in triplicates and repeated twice with different batch of cultures. Data represent mean ± SD of the values obtained from both experiments (**p < 0.01, *p < 0.05).

confirmed by PCR, sequencing (Fig. S1, supplementary data) and Southern blotting (Fig. 1B). One of the *M. bovis* Δ*sigF* mutants, Mb10, is described in this manuscript. The absence of SigF protein in Mb10 was confirmed by western blotting (Fig. 1C). The Mb10 mutant was complemented with the wild type *sigF* allele along with its native promoter in Mb11. The complementing cassette contained *sigF*, *rsbW* (anti-*sigF*) and the upstream *sigF* promoter, but the start codon of *rsbW* ORF was abrogated (Fig. S2, supplementary data), which allowed only functional copy of the SigF to be produced to complement the mutant. It may be noted that in Δ*sigF* mutant, while the *sigF* gene is disrupted, the functional copy of RsbW continues to be produced from its native promoter. Therefore, if the start codon of *rsbW* ORF is not abrogated in the complemented mutant strain the copy number of RsbW would increase and the stoichiometric balance between RsbW and SigF would be altered, leading to partial complementation of the Δ*sigF* mutant. It is important to note in this context that the overexpression of *rsbW* (anti-SigF) has been shown to produce *sigF* mutant like phenotype in *M. smegmatis* [12]. In present study, the *M. bovis* Δ*sigF* mutant and the complemented strain showed similar growth profile, akin to the wild type, in 7H9 liquid medium (Fig. 2). However, the Δ*sigF* mutant formed less aggregates than the wild type and grew as thinly spread colonies on LJ slants while the wild type and complemented strains formed thick

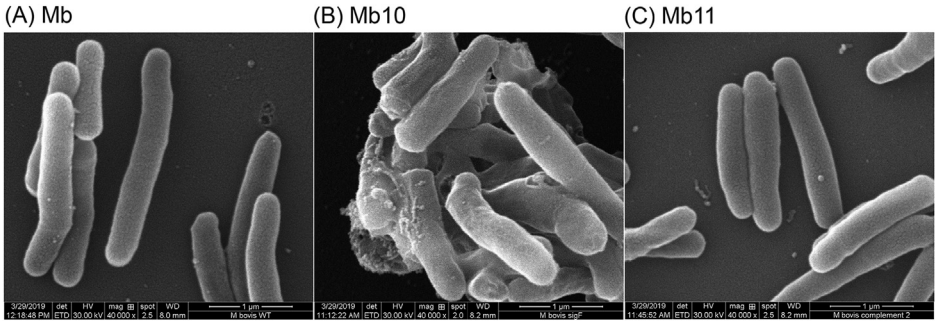

Fig. 5. Scanning electron micrograph images of *M. bovis* wild type (A), Δ*sigF* mutant (B) and complemented (C) strains. Release of extracellular material in the Δ*sigF* mutant relative to *M. bovis* wild type and complemented strain is evident. Pictures are at same resolution (1 μm).

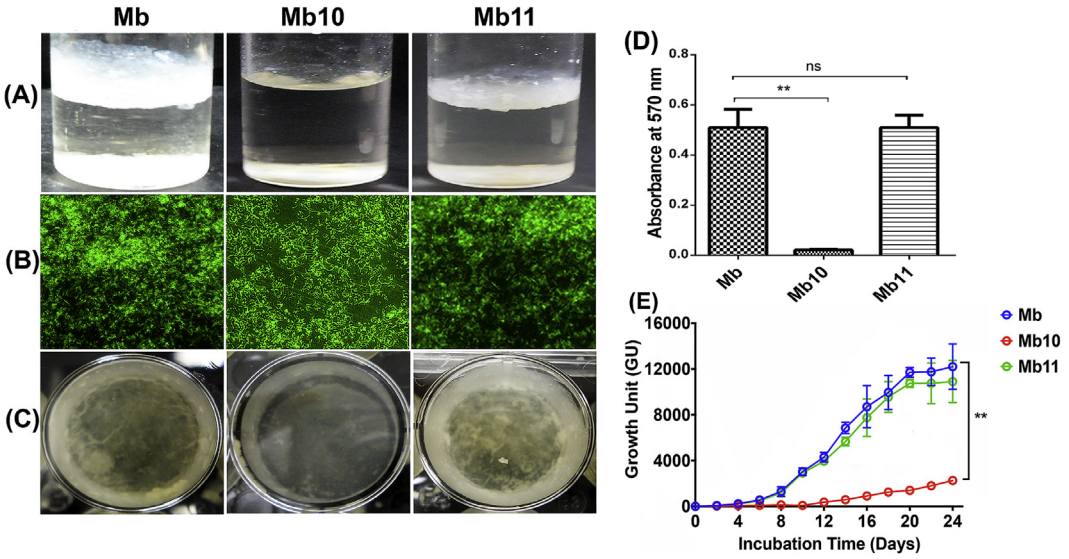

Fig. 6. *M. bovis* Δ*sigF* mutant (Mb10) exhibits deficiency in pellicles and biofilm formation in comparison to wild type (Mb) and complemented strain (Mb11). (A) Pellicle formation at air-liquid interface. (B) Pellicles of GFP expressing *M. bovis* strains were smeared - thinly distributed bacilli in apparently reduced biofilm matrix are evident in Mb10 mutant. (C) Biofilm formation in *M. bovis* strains. (D) Crystal violet staining for biofilm assessment. CV-stained biofilms were ethanol extracted and quantified by absorbance at 570 nm. The data are means ± SD of three wells per strain (**p < 0.01). (E) Biofilms from *M. bovis* wild type and complemented strain (Mb11) and non-biofilm forming Δ*sigF* mutant (Mb10) were treated with rifampicin (1 μg/ml) for 24 h. After treatment, cultures were washed and inoculated to MGIT960 vials. Treatment was done in duplicate and growth was monitored using BD MGIT 960 BACTEC system. Experiments were performed with two independent set of cultures and data at each time point represent mean ± SD (**p < 0.01 using paired *t*-test). Biofilm forming *M. bovis* wild type and complemented strain showed more resistance than the Δ*sigF* mutant (deficient in biofilms). (For interpretation of the references to colour in this figure legend, the reader is referred to the Web version of this article.)

growth (Fig. 3B). On 7H11 agar plates the wild type bacterial colonies displayed rough, highly textured spread out structure with twisting filaments or cords, while the Δ*sigF* mutant (Mb10) appeared smoother, less spread out with no visible filaments and cords (Fig. 3A). Wild type colony morphology was restored after complementing the mutant with *M. bovis sigF* (Mb11), suggesting that the change in colony morphotype was indeed due to *sigF* deletion. Colony morphology reflects even subtle changes in the cell wall components affecting the surface properties of the bacterial cells. Cell permeability was examined by measuring uptake of fluorescent dyes and susceptibility to antitubercular drugs. The Δ*sigF* mutant showed greater uptake of nile red and ethidium bromide (Fig. 3C and D) and increased susceptibility to the same concentration of antitubercular drugs (Fig. 4), indicating increased permeability of mutant bacteria with respect to wild type. Electron microscopy revealed normal morphology of the wild type *M. bovis* and the complemented strain while the Δ*sigF* mutant appeared distinct with pronounced presence of extracellular material surrounding the mutant cells (Fig. 5). The increasing amount of exudates around the mutant cells is most likely due to enhanced porosity of cell wall which further suggests the change in surface properties of the mutant cells.

***M. bovis* Δ*sigF* mutant displays defects in pellicles and biofilms formation.** Since the Δ*sigF* mutant colonies appeared strikingly different on agar plates and formed less aggregates than the wild type in liquid media, we examined if it is defective in pellicle formation. The Mb10 mutant failed to form pellicles under the same experimental conditions during which the parental strain showed thick pellicles (Fig. 6A). Next, we examined the mutant's ability to form biofilm. Recombinant *M. bovis* wild type, Δ*sigF* mutant and complemented strains expressing green fluorescent protein (GFP) constitutively from $hsp60_{pr}$ were grown in glass vials and allowed to develop pellicles. Subsequently, pellicles from air-liquid interface, thinly smeared on glass slides, were examined under FLoid® Cell Imaging Station (Thermo Fisher Scientific, India). Wild type bacterial colonies appeared as aggregates embedded in extracellular matrix of biofilm, while mutant bacteria were sparsely distributed in substantially reduced biofilm matrix (Fig. 6B). When cultures were grown in polystyrene plates, the mutant's reduced ability to form biofilm became more evident (Fig. 6C), which was consistent with the mutant's reduced ability to aggregate in liquid media or thick growth on LJ slants (Fig. 3B). Quantitative assessment of biofilm formation was performed by extracting the biofilm associated crystal violet dye [20]. Combined together, these results (Fig. 6B–D) clearly showed that the Δ*sigF* mutant exhibits reduced

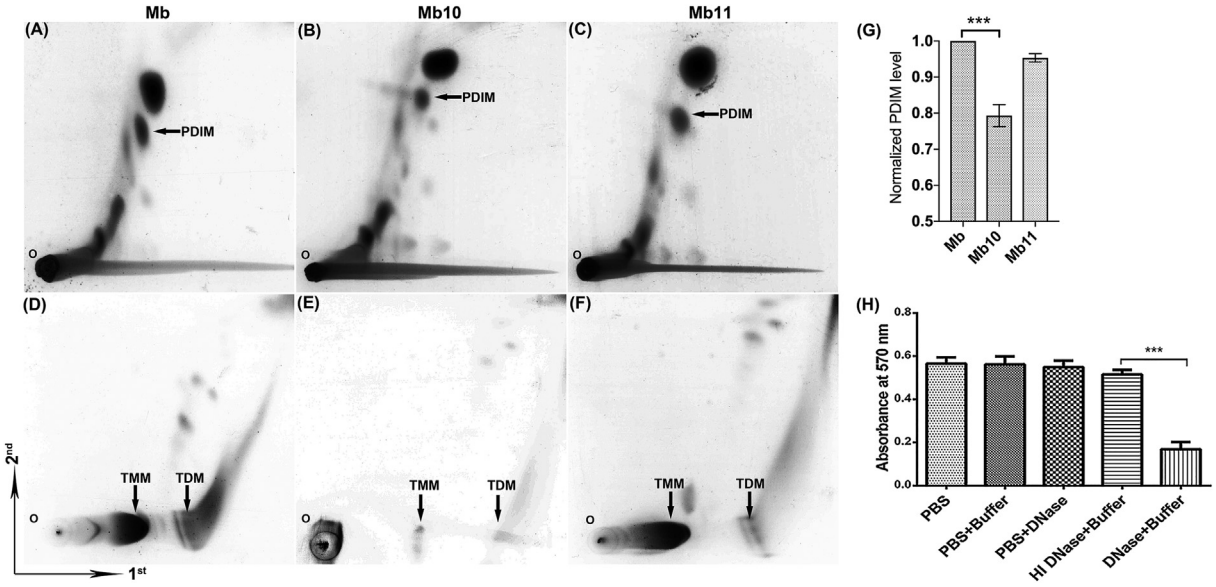

Fig. 7. 2D-TLC analysis of nonpolar lipids from *M. bovis* wild type (A), Δ*sigF* mutant (B) and complemented strain (C) and polar lipids from *M. bovis* wild type (D), Δ*sigF* mutant (E) and complemented strain (F). Different solvent systems, described in methods, were used to develop TLC plates. Arrows indicate the missing lipids in Mb10 Δ*sigF* mutant. PDIM- Phthiocerol dimycocerosate, TMM-Trehalose monomycolate, TDM-Trehalose dimycolate. **(G)** Quantitation of the PDIM level in different strains. PDIM spot (arrow) from panel A-C were scanned for densitometry using Image analysis software (GE Healthcare). The data were normalized to those for the wild-type strain. Data represent mean ± SD of the values obtained from three experiments with different batch of cultures (***p < 0.001). (H) DNase treatment disrupts biofilm formation in *M. bovis*. Plates carrying *M. bovis* wild type biofilms are incubated with PBS, PBS and reaction buffer, PBS and DNase, heat inactivated (HI) DNase and reaction buffer and DNase with reaction buffer. Biofilms are then quantified via crystal violet staining. Data represent mean ± SD of the values obtained from three independent experiments (***p < 0.001).

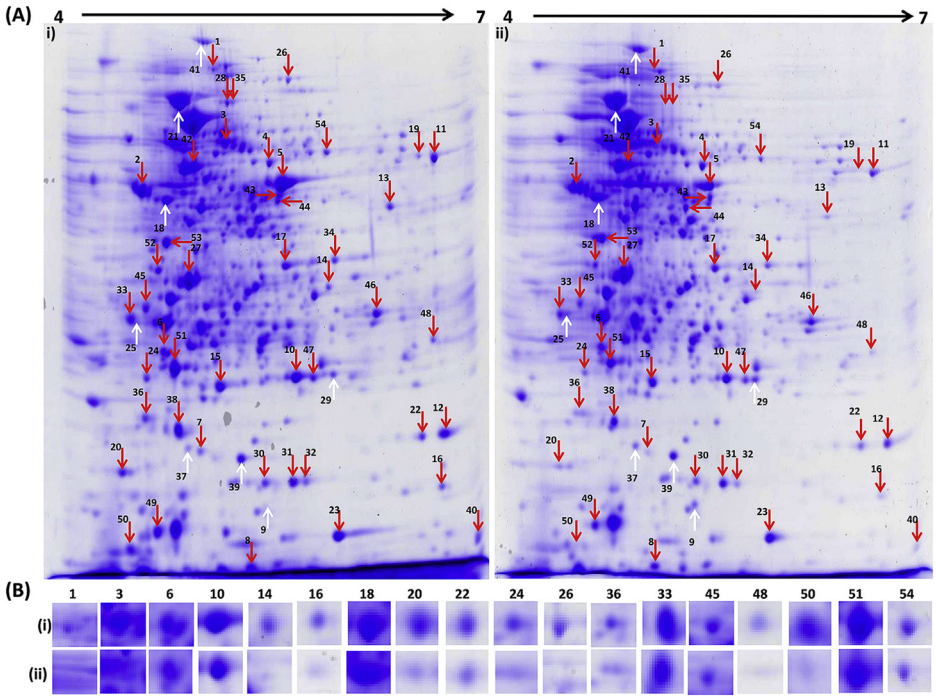

Fig. 8. (A) 2D profile of total proteins from stationary phase cultures of *M. bovis* wild type (i) and Δ*sigF* mutant (ii). Differentially regulated proteins (down-regulated - red arrows, up-regulated - white arrows) are marked with specific SPOT ID for MS-MS identification (Table 2). Panel B highlights the selected proteins spots from above gel pictures. This is a representative gel. (For interpretation of the references to colour in this figure legend, the reader is referred to the Web version of this article.)

ability to form biofilms in comparison to wild type under similar conditions. Complemented Δ*sigF* mutant restored the pellicle and biofilm formations, suggesting that these phenotypes are indeed due to *sigF* deletion in the mutant strain.

Lipids and DNA are integral to the biofilm. Organization of bacteria in biofilms is facilitated by self-produced extracellular matrix composed of mainly lipids and DNA (eDNA) [21]. The addition of DNase to cultures inhibits biofilm formation and dissolves mature biofilms. *M. bovis* biofilms were conspicuously disrupted by DNase treatment confirming the presence of eDNA in the biofilm matrix (Fig. 7H). To monitor changes in the lipids moieties, two-dimensional thin-layer chromatography (2D-TLC) was carried out for nonpolar and polar lipids extracted from *M. bovis* wild type, mutant and complemented bacterial cells, as described in the methods. Appreciable differences were noticed in trehalose 6-6′-dimycolate (TDM), the cord factor, trehalose 6-monomycolate (TMM) and phthiocerol dimycocerosate (PDIM) between the mutant and the wild type, which was largely restored in the complemented mutant strain (Fig. 7).

Table 2
Differentially regulated proteins of *M. bovis* Δ*sigF* mutant during stationary phase and *M. bovis* wild type strain during biofilm formation were identified by 2D-Gel Electrophoresis followed by MALDI-TOF MS/MS.

Spot ID	NCBI Accession Number	Protein Identified	Gene Theoretical	Masscot Score	Mass (kDa)	pI	Sequence Coverage%	Mtb orthologues	Fold-Change in Expression Δ*sigF*/wt
Down-regulated proteins									
1*	**gi|31793027**	Malate synthase	Mb1868c	94	80.58	5.03	3%	Rv1837c	0.01
2*	**gi|31792214**	Phosphopyruvate hydratase	Mb1051	890	44.99	4.50	28%	Rv1023	0.25
3	**gi|31793400**	Glutamine synthetase	Mb2244	606	53.70	4.84	34%	Rv2220	0.31
4	**gi|31792291**	Fumarate hydratase	Mb1128c	301	50.28	5.31	17%	Rv1098c	0.66
5*	gi|31791869	Elongation factor Tu	Mb0704	605	44.36	5.23	35%	Rv0685	0.36
6	**gi|31793740**	Hypothetical protein	Mb2587	605	24.67	4.80	44%	Rv2557	0.56
7*	**gi|31791537**	Hypothetical protein	Mb0367c	74	15.49	5.25	17%	Rv0360c	0.10
8	gi|31795087	Thioredoxin(Trx)	Mb3945	262	12.65	5.06	40%	Rv3914	0.54
10	**gi|31793741**	Hypothetical protein	Mb2588	229	26.04	6.18	26%	Rv2558	0.71
11*	**gi|31791420**	FabG	Mb0248c	308	46.91	6.04	22%	Rv0242c	0.62
12*	gi|31791186	PpiA	Mb0009	431	19.28	5.80	50%	Rv0009	0.52
13*	gi|31792674	MoxR1	Mb1515	622	40.71	5.89	39%	Rv1479	0.33
14	gi|31792394	Transferase	Mb1233c	299	32.79	5.59	30%	Rv1201c	0.14
15*	**gi|31791919**	Adenylate kinase (Adk)	Mb0754	177	20.11	5.02	18%	Rv0733	0.45
16	gi|31792348	Pyridoxamine 5′-phosphate oxidase	Mb1186	139	16.29	6.04	8%	Rv1155	0.33
17*	gi|31792648	Quinonereductase	Mb1489c	32	34.14	5.37	8%	Rv1454c	0.40
19*	gi|31792286	Serine hydroxymethyltransferase	Mb1123	170	45.05	6.12	18%	Rv1093	0.09
20*	**gi|31793124**	Thiol peroxidase (Tpx)	Mb1967	613	17.05	4.36	62%	Rv1932	0.48
22*	**gi|**31795020	Superoxide dismutase [Fe] SODA	Mb3876	448	23.02	5.96	30%	Rv3846	0.35
23	**gi|31792822**	Hypothetical protein (USP)	Mb1662	134	15.30	5.51	29%	Rv1636	0.81
24	gi|31793641	ATP-dependent Clp protease ClpP2	Mb2487c	243	23.58	4.99	28%	Rv2460c	0.59
26*	gi|31792048	Fatty oxidation protein FadB	Mb0883	915	76.17	5.42	25%	Rv0860	0.61
27*	**gi|31793325**	Wag31	Mb2169c	967	28.26	4.80	50%	Rv2145c	0.75
28	gi|31792501	F0F1 ATP synthase subunit alpha atpA	Mb1340	981	59.48	5.03	24%	Rv1308	0.31
30	**gi|31793214**	HspX	Mb2057c	552	16.08	5.00	64%	Rv2031c	0.66
31	**gi|31793214**	HspX	Mb2057c	203	16.08	5.00	64%	Rv2031c	0.82
32	gi|31793214	HspX	Mb2057c	335	16.08	5.00	64%	Rv2031c	0.75
33*	gi|31794207	Electron transfer flavoprotein fixA	Mb3055c	170	27.63	4.66		Rv3029c	0.21
34	gi|31793809	Hypothetical protein (USP)	Mb2656	504	31.74	5.46	39%	Rv2623	0.33
35*	gi|31791367	Dihydroxy-acid dehydratase	Mb0195c	29	59.77	5.06	2%	Rv0189c	0.22
36*	gi|31793017	Hypothetical protein(Cfp17)	Mb1858	88	17.24	4.29	9%	Rv1827	0.47
38	gi|31791231	Single-stranded DNA-binding protein	Mb0055	214	17.40	5.12	31%	Rv0054	0.31
40*	gi|31791820	HadB	Mb0655	99	14.92	6.08	24%	Rv0636	0.79
42	gi|31792503	ATP synthase F0F1 subunit beta AtpD	Mb1342	244	53.17	4.86	10%	Rv1310	0.42
43	gi|31794346	Hypothetical protein	Mb3194	381	41.84	5.28	29%	Rv3169	0.32
44	gi|31793426	3-oxoacyl-ACP synthase KasB	Mb2270	536	46.56	5.29	27%	Rv2246	0.54
45	**gi|31791823**	Transcription antiterminator NusG	Mb0658	532	25.43	4.70	36%	Rv0639	0.67
46	gi|31793918	Cytoplasmic protein, 35 kDa	Mb2765c	635	29.24	5.71	32%	Rv2744c	0.51
47	gi|31/793741	Hypothetical protein	Mb2588	737	26.04	6.18	52%	Rv2558	0.22
48	gi|31793341	F420-dependent oxidoreductase	Mb2185c	536	31.03	5.70	33%	Rv2161c	0.01
49	gi|31795048	ESAT-6-like protein EsxB	Mb3904	511	10.78	4.59	73%	Rv3874	0.33
50	**gi|31794599**	10 kDa chaperonin GroES	Mb3452c	193	10.94	4.87	42%	Rv3418c	0.09
51	**gi|31793077**	Secreted antigen 85-B FbpB	Mb1918c	348	30.81	4.87	25%	Rv1886c	0.50
52	**gi|31793809**	Hypothetical protein	Mb0854c	796	31.74	5.46	39%	Rv0831c	0.40
53	**gi|31792433**	Malate dehydrogenase	Mb1272	379	34.35	4.65	28%	Rv1240	0.22
54	gi|31791641	Lipoamide dehydrogenase	Mb0471	218	49.29	5.46	11%	Rv0462	0.58
Up-regulated proteins									
9	gi|31791429	Hsp induced ribosome-binding protein	Mb0257c	55	17.77	5.21	23%	Rv0251c	1.36
18	gi|31794633	RNA polymerase subunit alpha (RpoA)	Mb3486c	37	37.74	4.64	6%	Rv3457c	1.58
21	**gi|31791528**	Molecular chaperone	Mb0358	1382	66.79	4.85	31%	Rv0350	1.20
25	gi|31791759	Hypothetical protein (CFP32)	Mb0592	227	27.38	4.41	22%	Rv0577	1.27
29	gi|31791814	Enoyl-CoA hydratase (EchA3)	Mb0649c	118	24.45	5.52	31%	Rv0632c	1.40
37	gi|31792042	Hypothetical protein	Mb0877	128	16.33	5.10	18%	Rv0854	1.58
39	gi|31793320	Hypothetical protein	Mb2164c	346	18622	5.41	48%	Rv2140c	1.45
41	gi|31792670	Aconitate hydratase	Mb1511c	789	102.72	4.95	23%	Rv1475c	1.88

Protein spot IDs are same in 2D Gel images of *M. bovis* WT and Δ*sigF* mutant's stationary phase (Fig. 8) and in planktonic and biofilms culture (Fig. 9). Protein spot IDs/accession numbers in bold case refer to up-regulated proteins in *M. bovis* biofilms. Protein spot IDs marked with asterisk (*) refer to proteins whose genes harbor SigF consensus in their upstream regions (see Fig. 10B).

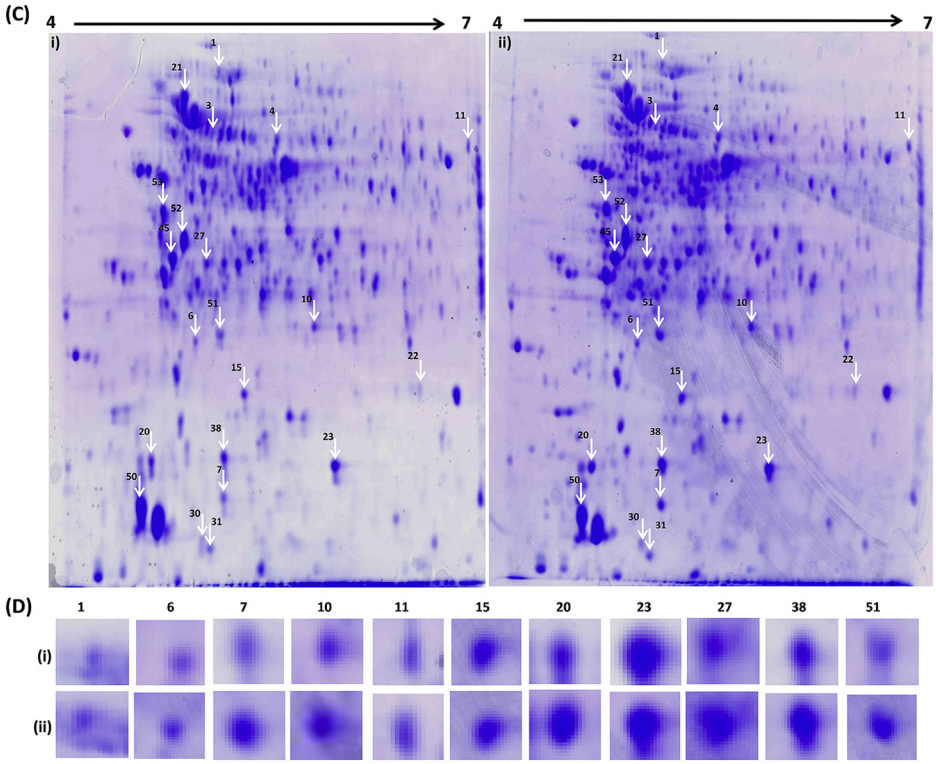

Fig. 9. (C) 2D profile of total proteins from *M. bovis* planktonic (i) and biofilms (ii). Most of the planktonic proteins appeared up-regulated in biofilms (white arrows). Panel D highlights the selected proteins spots from above gel pictures. Protein spot IDs are same in 2D Gel images of Figs. 8 (A) and 9 (C) panels. This is a representative gel.

Proteome analysis of *M. bovis* Δ*sigF* mutant and *M. bovis* biofilms. The proteome embodies the repertoire of proteins as expressed version of constituent genes and, therefore, its profiling provides an endpoint analysis of the observed phenotype elucidating the functional consequence of gene manipulation. To identify key proteins enabling the mutant's phenotype we performed comparative analyses of the mutant and the wild type proteome (Fig. 8). Since the *M. bovis* Δ*sigF* mutant was found to be deficient in biofilm formation, we analysed the proteins from *M. bovis* wild type strain during planktonic and biofilm stage. Several 2D gels were examined using ImageMaster™ 2D Platinum 7.0 (GE Healthcare). Proteins spots, which were consistent in different gels and showed significantly ($p < 0.05$) altered levels (Table 2) were considered for subsequent analysis by mass spectroscopy (see methods). Several proteins (e.g. Mb1868c, Mb1967, Mb2169c, Mb2656, Mb2587, Mb2588, Mb2487c) that appeared at lower levels in the Δ*sigF* mutant (Table 2) are reported to have functions that are consistent with their roles in pathogenesis and stress. Most of the proteins that were detected in planktonic stage were found to appear at higher levels in biofilms (Fig. 9). Moreover, proteins showing enhanced level in biofilms appeared down-regulated in *M. bovis* Δ*sigF* mutant (Table 2). One of the down-regulated proteins was malate synthase G (Mb1868c, *glcB*), a key enzyme of the glyoxylate pathway, which catalyzes the condensation of glyoxylate and acetyl-CoA to form malate. Interestingly, fumarate hydratase (Mb1128c), involved in the synthesis of malate from fumarate in TCA cycle, was also found to be diminished. Mb2487c encodes for ATP-dependent CLP protease (CLPP2) which is believed to have a role in pathogenicity [22]. Other proteins found to be reduced in the Δ*sigF* mutant are Wag31, which is reported to regulate growth, morphology and polar cell wall synthesis in *M. tuberculosis* [23], various transferases, transcriptional regulators, and other physiologically important proteins (Table 2). Some of the proteins were also found to be up-regulated, like Mb0358-a molecular chaperone, Mb3486c - RNA polymerase alpha subunit, Mb0257c- Hsp induced ribosome-binding protein and other hypothetical proteins (Fig. 8, Table 2). Expressions of some of the genes encoding proteins that were down-regulated in the Δ*sigF* mutant were validated by real-time qRT-PCR. Similar to proteome profile, the selected genes showed reduced expressions in real-time PCR (Fig. 10A). Many genes encoding for these proteins possess SigF consensus in their upstream regions suggesting that they are, possibly, SigF-dependent (Fig. 10B). The others could be indirectly regulated by SigF.

***M. bovis* Δ*sigF* mutant (MB10) showed compromised pathogenesis.** To investigate the role of SigF in pathogenicity of *M. bovis*, we investigated the *in vivo* growth phenotype of the Mb10 mutant in BALB/c mouse model by time-to-death analysis. Groups of BALB/c mice were infected intravenously with *M. bovis* wild type, Mb10 mutant, and complemented (Mb11) mutant. Bacterial intake was confirmed by sacrificing three animals from each group 24 h post-infection and by enumerating CFUs from lung homogenate on 7H11 agar plates. Despite receiving almost equal bacteria doses (~5.6 $\log_{10}$ CFUs) of different *M. bovis* strains (Fig. 11A), mice infected with *M. bovis* and complemented mutant lost weight noticeably after 40 days in comparison to animals infected with Mb10 mutant (Fig. 11B). In time-to-death analysis, animals infected with Mb10 mutant survived more (median survival: 210 days) than the animals infected with the wild type and complemented mutant (median survival time: 90 days) (Fig. 11C). These data suggest that the *sigF* mutant exhibits less virulence and disease progression in this BALB/c mouse model. To monitor degree of infection, disease progression and bacterial burden, the lungs and spleens were removed aseptically at defined time intervals and organ homogenates serially-diluted and plated on 7H11 agar and CFUs enumerated following incubation (Fig. 11D and E). The Mb10 mutant was found to be attenuated for growth in the mouse lungs as well as the spleen across the time points (Fig. 11D and E). In case of mice infected with the complemented strain, CFUs in lungs and spleen nearly matched wild type across all time points.

It was shown that in *M. tuberculosis* malate synthase is secreted extracellularly, localizes on the mycobacterial cell wall and enhances the adherence of bacteria to lung epithelial A549 cells [19]). To examine this, we incubated the *M. bovis* wild type, Δ*sigF* mutant and complemented strains with A549 cells and examined the binding by endpoint CFU analysis (Fig. 12A). At both the low (10:1) and high

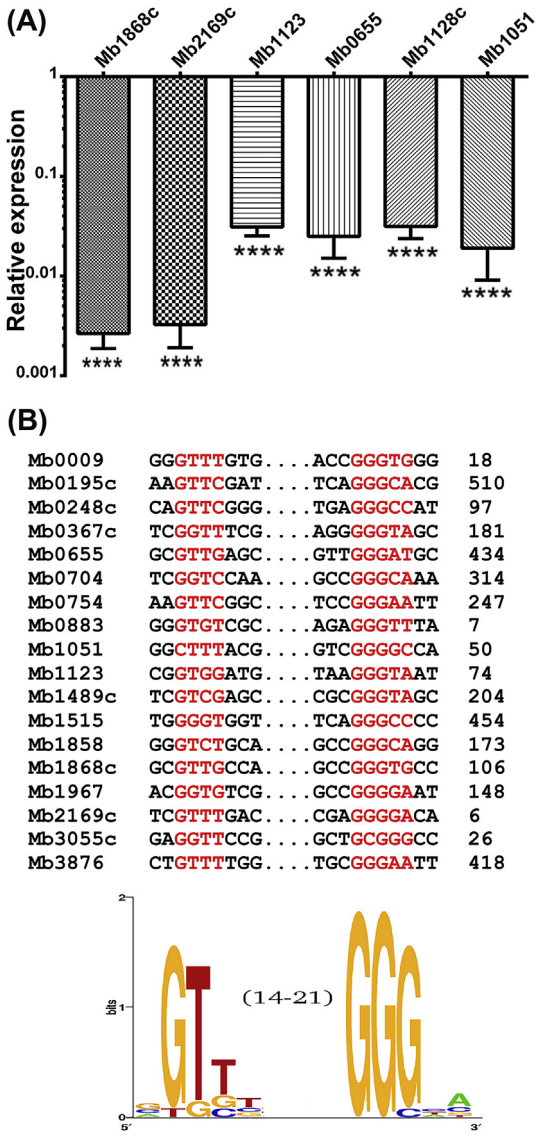

Fig. 10. Validation of differentially regulated proteins. (A) Relative expressions of select genes were determined from the RNA samples isolated from *M. bovis* wild type (Mb) and Δ*sigF* mutant (Mb10) culture. Expression of genes was normalized with the *sigA* transcript level. Similar to proteome analysis expression of these genes appeared down-regulated in the Δ*sigF* mutant. The mean value and standard deviations were calculated from two different experiments using RNAs from two different batches of cultures and significance (****$p < 0.0001$) was determined using One-way ANOVA, Brown-Forsythe test. (B) SigF binding consensus sequences (−10 and −35 regions shown in red) were identified in the upstream of SigF regulated genes. The distance in nucleotides of −10 regions from the annotated initiation codon is shown on right side. Graphical representation of SigF consensus was generated using Web logo tool. (For interpretation of the references to colour in this figure legend, the reader is referred to the Web version of this article.)

(100:1) multiplicity of infection (moi) tested, around 6% of input inocula of *M. bovis* wild type bound to cell surface, while there was a visible decline (3-4%) in adherence of the Δ*sigF* mutant. Concomitant with this, low level of malate synthase was apparent in Mb10 mutant in comparison to the wild type and the complemented strain (Fig. 12B). To further ensure that the decline in adherence is due to diminished level of malate synthase in the Δ*sigF* mutant, we created a merodiploid strain (MB10/MS) with the malate synthase gene (Mb1868c) under transcriptional control of *hsp60* promoter. This allowed the expression of Mb1868c independent of SigF and compensated the loss of malate synthase incurred due to *sigF* deletion. The merodiploid strain restored the loss in adherence (Fig. 12 A), indicating that the down-regulation of malate synthase in the mutant, most likely, resulted in reduced adherence of mutant bacilli to epithelial cells.

4. Discussion

Initially SigF was deemed a stationary-phase stress-response sigma factor present only in slow-growing mycobacterial species whose inappropriate overexpression is incompatible with growth in *M. bovis* BCG [3]. Later with availability of mycobacterial whole genome sequences and in our own studies, SigF was found to be widely conserved in mycobacteria except its pseudogenization in *M. leprae* [4,5]. In BALB/c mouse model the *M. tuberculosis* Δ*sigF* mutant replicates in lung at lower bacterial burdens than wild type and was found to be attenuated in terms of the disease pathogenesis [6,7]. In non-tuberculous, fast-growing mycobacteria, *sigF* is widely expressed during growth, suggesting its larger role in mycobacteria apart from regulation of virulence genes in *M. tuberculosis* [11,12]. Genome-wide gene expression studies using *sigF* mutant of *M. tuberculosis* H37Rv and CDC1551 strains and few other studies showed that the SigF regulon largely comprises genes with predicted roles in cell wall synthesis, stress response and virulence [7,9,10]. Characterization of SigF regulon in *M. smegmatis* identified genes with predicted roles in oxidative stress, stationary phase adaptation and in maintenance of cell wall architecture [11,12]. Most of these studies were based on transcription analysis. A proteome-based regulon analysis of a Δ*sigF* mutant in any mycobacterial species was lacking as was a detailed analysis of the cellular and colony morphotype of a Δ*sigF* mutant and its surface properties, considering the implications of genes in the SigF regulon.

In this study, we generated a *sigF* null mutant in *M. bovis* and studied its surface phenotypes and proteome. While the wild type *M. bovis* strain formed typical rough colonies with highly textured surface and irregularly spread margins, the Δ*sigF* mutant produced smooth colonies without protruded margins. Colony morphotypes in mycobacteria have been associated with surface properties like pellicle and biofilm formation [24,25]. Consistent with this, wild type *M. bovis* colonies formed a thick pellicle over the entire surface of the medium while the mutant strain showed greatly reduced tendency to spread and did not coalesce forming noticeable pellicles (Fig. 6A). Examination of the surface pellicles revealed that the wild type rough morphotype formed thick aggregates that stayed embedded in extracellular matrix poorly constituted in the *sigF* mutant. Thus, the differences in the appearance on the surface of liquid medium are reflections of the same basic differences observed on solid agar media. Pellicle and biofilm formation are contributed by various lipid moieties that enrich the mycobacterial cell wall. Free mycolic acids (FM) have been shown to be a major component of the extracellular matrix and a facilitator of biofilm formation in mycobacteria [14]. One of the precursors for FM is newly synthesized TDM, the most abundant lipid in *M. tuberculosis* [26]. Synthesis of mycolic acids leading to formation of TMM occurs in the cytoplasm and TMM is transported across the cytoplasmic membrane where it serves as a precursor for TDM synthesis. TDM forms the major component of mycobacterial cell envelope and its exudates. It forms a crystalline monolayer at air-liquid interface that is exceedingly stable, rigid and potentially capable of supporting a pellicle of organisms [26]. The *sigF* mutant showed diminished level of TDM and TMM and apparently failed to form pellicles at air-liquid interface. Pellicles at air-liquid interface are basically enriched biofilms embedded in extracellular matrix. Self-organization of bacterial biofilms is facilitated by extracellular DNA (eDNA) as the presence of eDNA in biofilm matrix rendered stability to the biofilms [27]. We confirmed the presence of eDNA in *M. bovis* biofilms. eDNA has been shown to be a major component of the extracellular matrix that supports the expression of drug tolerant bacilli [28]. This mode of life confers several advantages to bacteria over planktonic mode of existence as biofilms render more resistance to

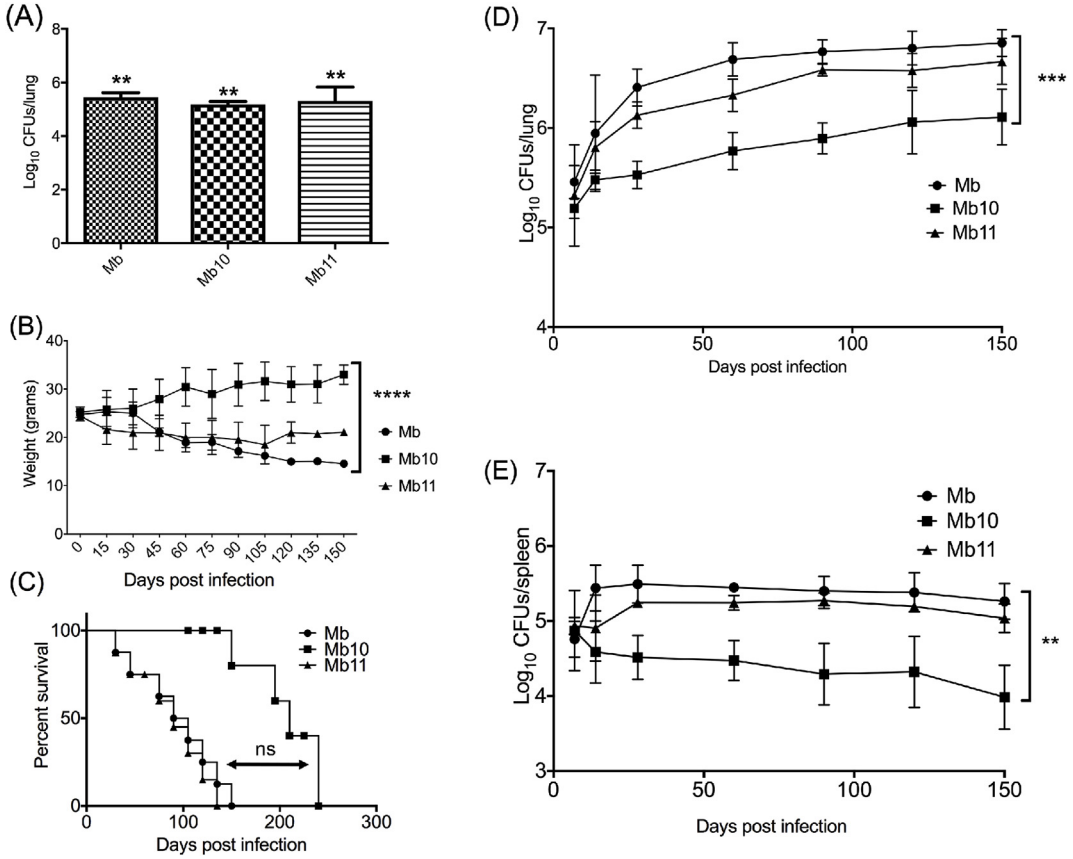

Fig. 11. *In vivo* characterization of *M. bovis* Δ*sigF* mutant (Mb10). (A) Implantation of *M. bovis* wild type (Mb), Δ*sigF* mutant (Mb10), complemented (Mb11) strains in BALB/c mice. Three animals from each group were sacrificed after 24 h of infection, CFU was enumerated and average CFU of lung homogenate of each group was plotted with ± SD (**p < 0.01). (B) Weights of animals in study group were recorded biweekly and average weight was plotted with ± SD (****p < 0.0001). (C) Time-to-death analysis of infected mice showed enhanced survival of mice infected with *sigF* mutants in comparison to mice infected with wild type and complemented strains. The results are presented as percent survival and the significance was determined using log-rank Mantel-Cox tests (ns, nonsignificant). Growth and proliferation of *M. bovis* wild type, Δ*sigF* mutant and complemented strains in lungs (D) and spleen (E). Three animals from each group of infected mice were sacrificed at specific time interval and numbers of bacteria in lungs and spleen were enumerated. The results for each time point represent mean CFU ± SD of organs from three animals. The statistical significance was determined using two tailed paired *t*-test (**p < 0.01, ***p < 0.001).

antibiotics than planktonic cells. Notably, the Δ*sigF* mutant showed significantly reduced tolerance to antitubercular drugs in comparison to wild type bacilli (Fig. 4 B-D, 6E). The formation of biofilms inside a host confers advantages as biofilms help repopulate colonized sites providing reservoir of cells after withdrawal of drug treatment, thereby, making the treatment extremely difficult. In *M. tuberculosis* infected guinea pigs, after drug treatment, the surviving population of the pathogen was found to be in microcolonies located around the acellular rim of the granulomas [29]. Thus, the biofilm formation appears an effective and ubiquitous strategy that helps pathogen proliferate as a stress-tolerant community in a host. As we demonstrate that the SigF facilitates biofilm formation in *M. bovis* and that the *sigF* mutant is deficient in biofilm formation and other surface properties, SigF is likely to play important role in pathogenesis of mycobacteria by regulating bacterial assembly and networking of biofilms.

The changes in mycobacterial colony morphologies have been linked with altered virulence [30]. In *Mycobacterium abscessus*, comparative analysis of rough and smooth colony variants showed that the rough morphotype tends to be more virulent in experimental infection models [24]. The *M. bovis* Δ*sigF* mutant survived and produced sustained bacterial burden in mouse tissues, but is attenuated. This pattern of attenuation with high lung CFU counts, but delayed time-to-death results have been earlier observed in other mycobacterial alternative sigma factor mutants, e.g. *M. tuberculosis* Δ*sigH* [31], Δ*sigE* [32] and Δ*sigC* [33]. The TDM has been reported to contribute to rough colony morphotype associated with virulence [26]. *M. tuberculosis* with TDM removed remained viable but failed to induce progressive infections when injected into mice [34]. Removal of TDM from the surface of BCG has been shown to reduce its ability to persist in the lungs and spleens of mice following intravenous injection [35]. TDM has been shown to induce granulomatous response in animal models [36,37] and mutants defective in cording showed loss of lethal chronic persistence in mice, suggesting a strong correlation between cords, rough colonial morphology and increased persistence of mycobacteria inside macrophages [38]. Another surface lipid, phthiocerol dimycolate (PDIM), has also been reported as important virulence factor, as PDIM-deficient *M. tuberculosis* exhibited growth defects and reduced bacterial load in a mouse model [39]. Importantly, mice infected with the *sigF* mutant showed reduced bacterial burden and enhanced survival time in comparison to mice infected with *M. bovis* wild type and complemented *sigF* mutant strains. Considering this, it is tempting to speculate that the changed surface properties and *in vivo* phenotypes of compromised pathogenesis exhibited by the *sigF* mutant could be due to alterations in these lipid moieties in the mutant.

Altered surface properties of the Δ*sigF* mutant corroborated well with the findings from proteome analysis. Since the *sigF* is largely expressed in the stationary phase of *M. bovis*, we analysed the proteins from stationary phase cells [5]. Several proteins that showed reduced level in the Δ*sigF* mutant were found to be elevated in *M. bovis* biofilms, highlighting the role of SigF in the biofilm formation. One of the reduced proteins was malate synthase G (MSG), which was confirmed by western analysis (Fig. 12B) and its transcriptional down-regulation was

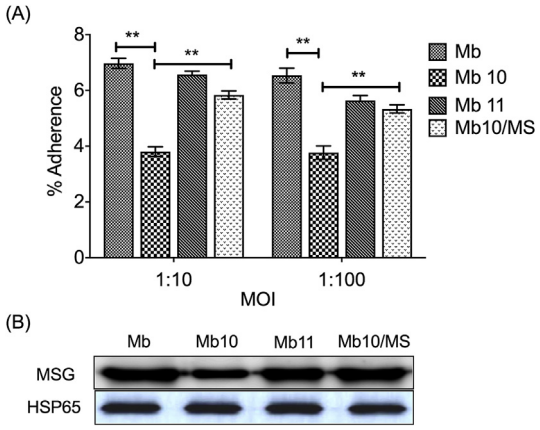

Fig. 12. (A) Adherence assay was performed using *M. bovis* wild type (Mb), Δ*sigF* mutant (Mb10), complemented strain (Mb11) and merodiploid strain Mb10/MS (Mb10 transformed with *M. bovis* malate synthase gene) and lung epithelial cells (A549). Percent adherence was determined as described in methods. Experiment was performed twice with different batch of cultures and three technical replicates in each set. Data represent means ± SD using paired *t*-test (**p < 0.01). (B) Western blot analysis of total proteins from stationary phase cultures of *M. bovis* wild type (Mb), Δ*sigF* mutant (Mb10) and complemented strain (Mb11) and merodiploid strain Mb10/MS using malate synthase antibody [46]. Proteins were detected with rabbit anti-MSG antibody (1:100), followed by goat anti-rabbit HRP antibody (Sigma) (1:40000). Consistent with proteome and real-time data, low level of malate synthase was detected in Δ*sigF* mutant (Mb10). For uniformity in loading of proteins blot was probed with mouse anti-HSP65 antibody (Santa Cruz).

confirmed in the Δ*sigF* mutant (Fig. 10A). The malate synthase G allows bacteria to assimilate two carbon compounds into the TCA cycle and is utilized by *M. tuberculosis* while replicating in host macrophages [40]. In addition to this, MSG has been reported to be secreted, anchored on the bacterial cell wall, where, it enhances the adherence of bacteria to lung epithelial cells. When secreted to surface, MSG binds to laminin and fibronectin as adhesive and promotes self aggregation to form biofilms [19]. In view of this fact and conforming to the significant down-regulation of MSG gene in the Δ*sigF* mutant, reduced attachment to A549 cells by the Δ*sigF* mutant was observed compared to wild type *M. bovis*. Reduced adherence may well result from the different surface lipid composition by the mutant. To demonstrate that the down regulation of malate synthase gene resulted in reduced adherence of the mutant to epithelial cells, we transformed the Δ*sigF* mutant with the malate synthase gene under transcriptional control of a promoter independent of SigF. This strain partially restored adherence (Fig. 12A), confirming the role of malate synthase in the adherence of *M. bovis* bacilli to lung epithelial cells. Other proteins that were found to be significantly reduced in Mb10 mutant included: a CLP protease (Mb2487c), CFP32 (Mb0592), TpX (Mb1967), Wag31 (Mb2169c), two co-existing hypothetical proteins (Mb2587-2588), MoxR (Mb1515), SodA (Mb3876), a putative ATP-binding protein (Mb2656) and others (see Table 2). The Mb2487c ortholog in *M. tuberculosis* (Rv2460c) encodes for ATP-dependent CLP protease which is conserved in *M. tuberculosis*, *M. leprae*, *M. bovis* and *M. avium paratuberculosis*. This has been predicted to be essential for *in vivo* survival and pathogenicity [22]. Mb0592 encoding CFP32 (Rv0577), a putative glyoxalase, is restricted to *M. tuberculosis* complex (MTC) members, and has been detected in pulmonary tuberculosis patients, implicating its role in tuberculosis pathogenicity [41]. Two hypothetical proteins from *M. bovis* (Mb2587, Mb2588) and their orthologs in *M. tuberculosis* (Rv2557, Rv2558) are found to be syntenic. In *M. tuberculosis*, genes encoding these proteins were co-expressed and their transcripts were detected in human lung necrotic granulomas [42]. It was hypothesized that the expression of these genes is required during the adaptive response of the bacilli from an intracellular to a more hostile extracellular necrotic environment [42]. Both, Mb2587 and Mb2588 were found to be down-regulated in the *sigF* mutant. Wag31 (Mb2169c/Rv2145c) has been reported to interact with AccA3, involved in lipid biosynthesis, cell wall lipid permeability and lipophilic drug resistance in *M. smegmatis* [43]. Using co-immunoprecipitation analysis, it was shown that, six proteins (AccA3, AccD4, AccD5, Fas, InhA and MmpL3) that are involved in fatty acid and mycolic acid synthesis belong to the Wag31 interactome [43]. Wag31 knock-down in *M. smegmatis* resulted in an increased cellular permeability to lipophilic molecules as this led to higher accumulation of the lipophilic Nile red dye in the cytoplasm [43]. In this study, we identified the SigF footprints in the upstream region of *wag31* (Mb2169c) (Fig. 10B) and showed that it is down regulated in the Δ*sigF* mutant (Fig. 10A), which suggests that the *wag31* is transcriptionally regulated by SigF. It may be recalled that the Δ*sigF* mutant also showed enhanced permeability to lipophilic Nile red dye. Another reduced protein, encoded by Mb2656, is a putative ATP-binding protein while its *M. tuberculosis* homolog (Rv2623) encodes a universal stress protein. In *M. tuberculosis*, Rv2623 is among the most highly induced genes when the tubercle bacillus is subjected to hypoxia and inside macrophages during chronic tuberculosis [44,45]. Rv2623 deletion mutant failed to establish chronic tuberculous infection in guinea pigs and mice [45].

The SigF regulon has been deduced earlier using transcriptome-based analyses in *M. tuberculosis* strains H37Rv and CDC1551 [7,9,10]. In these studies, the overlap of genes reported to be SigF dependent was quite small, possibly, due to different physiological traits of these strains or due to change in experimental conditions affecting the impact of sigma factors in global gene regulation. In this study, since we studied proteins, the observed differences in SigF dependent genes with those identified earlier by transcriptome analysis were, expectedly, large. Nevertheless, diminished levels of several of these proteins, having the proven roles in the pathogenesis, most likely, would have been the reason for the reduced pathogenicity and lower bacterial burden in animals infected with the *M. bovis* Δ*sigF* mutant.

In summary, we have shown that the SigF regulon comprises genes that regulate the surface properties of mycobacteria, as *sigF* mutant showed deficiency in biofilm, pellicle and cord formation. The most abundant cell wall lipid and key cord forming molecule, TDM, was barely detectable in the Δ*sigF* mutant. Deletion of *sigF* resulted in significant down-regulation of several proteins with predicted roles in cell wall biosynthesis, stress response and virulence associated functions. The lower levels of malate synthase in the Δ*sigF* mutant affecting adherence properties of bacilli to lung epithelial cells fortified the pleiotropic role of this housekeeping enzyme adding to the increasing repertoire of the SigF regulon. These findings will help improve our understanding of the role of SigF in mycobacterial biology.

Conflicts of interest

The authors declare no conflict of interest.

Acknowledgments

We are extremely grateful to late Jean-Mark Reyrat, University of Paris for providing pPR27 allele exchange vector. The malate synthase antibody was a kind gift from Dr Sudheer Singh, Principal scientist from Microbiology Division, CDRI. Debashis, Vishal and Ashutosh received their junior and senior research fellowships from CSIR, ICMR and UGC, respectively. The work was supported by CSIR Network Project BSC0111 awarded to Bhupendra N. Singh. This is manuscript No. 9869 of CDRI.

Appendix A. Supplementary data

Supplementary data to this article can be found online at https://doi.org/10.1016/j.tube.2019.07.006.

References

[1] Forrellad MA, Klepp LI, Gioffré A, Sabio YGJ, Morbidoni HR, de la Paz Santangelo M, Cataldi AA, Bigi F. Virulence factors of the *Mycobacterium tuberculosis* complex. Virulence 2013;4:3–66.

[2] Garnier T, Eiglmeier K, Camus J-C, Medina N, Mansoor H, Pryor M, Duthoy S, Grondin S, Lacroix C, Monsempe C, Simon S, Harris B, Atkin R, Doggett R, Mayes R, Keating L, Wheeler PR, Parkhill J, Barrell BG, Cole ST, Gordon SV, Hewinson RG R. The complete genome sequence of *Mycobacterium bovis*. Proc Natl Acad Sci USA 2003;100:7877–82.

[3] DeMaio J, Zhang Y, Ko C, Young DB, Bishai WR. A stationary-phase stress-response sigma factor from *Mycobacterium tuberculosis*. Proc Natl Acad Sci USA 1996;93:2790–4.

[4] Waagmeester A, Thompson J, Reyrat J-M. Identifying sigma factors in *M. smegmatis* by comparative genomic analysis. Trends Microbiol 2005;13:505–9.

[5] Singh AK, Singh BN. Conservation of sigma F in mycobacteria and its expression in *Mycobacterium smegmatis*. Curr Microbiol 2008;56:574–80.

[6] Chen P, Ruiz RE, Li Q, Silver RF, Bishai WR. Construction and characterization of a *Mycobacterium tuberculosis* mutant lacking the alternate sigma factor gene, *sigF*. Infect Immun 2000;68:5575–80.

[7] Geiman DE, Kausha D, Tyagi S, Manabe YC, Schroeder BG, Fleischmann RD, Morrison NE, Converse PJ, Chen P, Bishai WR. Attenuation of late-Stage disease in mice infected by the *M. tuberculosis* mutant lacking the *sigF* alternate sigma factor and identification of SigF-dependent genes by microarray analysis. Infect Immun 2004;72:1733–45.

[8] Gebhard S, Hümpel A, McLellan AD, Cook GM. The alternative sigma factor SigF of *Mycobacterium smegmatis* is required for survival of heat shock, acidic pH and oxidative stress. Microbiology 2008;154:2786–95.

[9] Hartkoorn RC, Sala C, Uplekar S, Busso P, Rougemont J, Cole ST. Genome-wide definition of the SigF regulon in *Mycobacterium tuberculosis*. J Bacteriol 2012;194:2001–9.

[10] Williams EP, Lee J-H, Bishai WR, Colantuoni C, Karakousis PC. *Mycobacterium tuberculosis* SigF regulates genes encoding cell wall-associated proteins and directly regulates the transcriptional regulatory gene phoY1. J Bacteriol 2007;189:4234–42.

[11] Hümpe A, Gebhard S, Cook GM, Berney M. The SigF regulon in *Mycobacterium smegmatis* reveals roles in adaptation to stationary phase, heat, and oxidative Stress. J Bacteriol 2010;192. 2491-02.

[12] Singh AK, Dutta D, Singh V, Srivastava V, Biswas RK, Singh BN. Characterization of *Mycobacterium smegmatis sigF* mutant and its regulon: overexpression of SigF antagonist (MSMEG_1803) in *Mycobacterium smegmatis* mimics *sigF* mutant phenotype, loss of pigmentation and sensitivity to oxidative stress. MicobiologyOpen 2015;4. 896-16.

[13] Sambrook J, Fritsch EF, Maniatis T. Molecular Cloning: a laboratory manual. second ed. NY: Cold Spring Harbor Laboratory Press, Cold Spring Harbor; 1989.

[14] Ojha AK, Baughn AD, Sambandan D, Hsu T, Trivelli X, Guerardel Y, Alahari A, Kremer L, Jacobs Jr. WR, Hatfull GF. Growth of *Mycobacterium tuberculosis* biofilms containing free mycolic acids and harbouring drug-tolerant bacteria. Mol Microbiol 2008;69:164–74.

[15] López D, Vlamakis H, Kolter R. Biofilms. Cold Spring Harb Perspect Biol. 2010;2. a000398.

[16] Yu J, Tran V, Li M, Huang X, Niu C, Wang D, Zhu J, Wang J, Gao Q, Liu J. Both phthiocerol dimycocerosates and phenolic glycolipids are required for virulence of *Mycobacterium marinum*. Infect Immun 2012;80:1381–9.

[17] Shevchenko A, Tomas H, Havlis J, Olsen JV, Mann M. In-gel digestion for mass spectrometric characterization of proteins and proteomes. Nat Protoc 2006;1:2856–60.

[18] Singh AK, Singh BN. Differential expression of *sigH* paralogs during growth and under different stress conditions in *Mycobacterium smegmatis*. J Bacteriol 2009;191:2888–93.

[19] Kinhikar AG, Vargas D, Li H, Mahaffey SB, Hinds L, Belisle JT, Laal S. *Mycobacterium tuberculosis* malate synthase is a laminin-binding adhesin. Mol Microbiol 2006;60. 999-13.

[20] Carte G, Wu M, Drummond DC, Bermudez LE. Characterization of biofilm formation by clinical isolates of *Mycobacterium avium*. J Med Microbiol 2003;52:747–52.

[21] Gloag ES, Turnbull L, Huang A, Vallotton P, Wang H, Nolan LM, Mililli L, Hunt C, Lu J, Osvath SR, Monahan LG, Cavaliere R, Charles IG, Wand MP, Gee ML, Prabhakar R, Whitchurch CB. Self-organization of bacterial biofilms is facilitated by extracellular DNA. Proc Natl Acad Sci USA 2013;110:11541–6.

[22] Ribeiro-Guimarães ML, Pessolani MC. Comparative genomics of mycobacterial proteases. Microb Pathog 2007;43:173–8.

[23] Kang CM, Nyayapathy S, Lee JY, Suh JW, Husson RN. Wag31, a homologue of the cell division protein DivIVA, regulates growth, morphology and polar cell wall synthesis in mycobacteria. Microbiology 2008;154:725–35.

[24] Howard ST, Rhoades E, Recht J, Pang X, Alsup A, Kolte R, Lyons R, Byrd TF. Spontaneous reversion of *Mycobacterium abscessus* from a smooth to a rough morphotype is associated with reduced expression of glycopeptidolipid and reacquisition of an invasive phenotype. Microbiology 2006;152:1581–90.

[25] Fregnan GB, Smith DW. Description of various colony forms of mycobacteria. J Bacteriol 1962;83:819–26.

[26] Hunter RL, Venkataprasad N, Olsen MR. The role of trehalose dimycolate (cord factor) on morphology of virulent *M. tuberculosis* in vitro. Tuberculosis 2006;86:349–56.

[27] Whitchurch CB, Tolker-Nielsen T, Raga PC, Mattick JS. Extracellular DNA required for bacterial biofilm formation. Science 2002;295:1487.

[28] Ryan GJ, Hoff DR, Driver ER, Voskuil MI, Gonzalez-Juarrero M, Basaraba RJ, Crick DC, Spencer JS, Lenaerts AJ. Multiple *M. tuberculosis* phenotypes in mouse and Guinea pig lung tissue revealed by a dual-staining approach. PLoS One 2010;5:e11108.

[29] Lenaerts AJ, Hoff D, Aly S, Ehlers S, Andries K, Cantarero L, Orme IM, Basaraba RJ. Location of persisting mycobacteria in a Guinea pig model of tuberculosis revealed by r207910. Antimicrob Agents Chemother 2007;51:3338–45.

[30] Kansal RG, Gomez-Flores R, Mehta RT. Change in colony morphology influences the virulence as well as the biochemical properties of the *Mycobacterium avium* complex. Microb Pathog 1998;25:203–14.

[31] Kaushal D, Schroeder BG, Tyagi S, Yoshimatsu T, Scott C, Ko C, Carpenter L, Mehrotra J, Manabe YC, Fleischmann RD, Bishai WR. Reduced immunopathology and mortality despite tissue persistence in a *Mycobacterium tuberculosis* mutant lacking alternative sigma factor, SigH. Proc Natl Acad Sci USA 2002;99:8330–5.

[32] Ando M, Yoshimatsu T, Ko C, Converse PJ, Bishai WR. Deletion of *Mycobacterium tuberculosis* sigma factor E results in delayed time to death with bacterial persistence in the lungs of aerosol-infected mice. Infect Immun 2003;71:7170–2.

[33] Sun R, Converse PJ, Ko C, Tyagi S, Morrison NE, Bishai WR. *Mycobacterium tuberculosis* ECF sigma factor sigC is required for lethality in mice and for the conditional expression of a defined gene set. Mol Microbiol 2004;52:25–38.

[34] Kan-Sutton C, Jagannath C, Hunter Jr. RL. Trehalose 6,6'-dimycolate on the surface of *Mycobacterium tuberculosis* modulates surface marker expression for antigen presentation and costimulation in murine macrophages. Microb Infect 2009;11:40–8.

[35] Silva CL, Ekizlerian SM, Fazioli RA. Role of cord factor in the modulation of infection caused by mycobacteria. Am J Pathol 1985;118:238–47.

[36] Hunter RL, Olsen M, Jagannath C, Actor JK. Trehalose 6,6'-dimycolate and lipid in the pathogenesis of caseating granulomas of tuberculosis in mice. Am J Pathol 2006;168:1249–61.

[37] Geisel RE, Sakamoto K, Russell DG, Rhoades ER. In vivo activity of released cell wall lipids of *Mycobacterium bovis* BCG is due principally to trehalose mycolates. J Immunol 2005;174:5007–15.

[38] Glickman MS, Cox JS, Jacobs WR. A novel mycolic acid cyclopropane synthetase is required for cording, persistence, and virulence of *M. tuberculosis*. Mol Cell 2000;5:717–27.

[39] Day TA, Mittler JE, Nixon MR, Thompson C, Miner MD, Hickey MJ, Liao RP, Pang JM, Shayakhmetov DM, Sherman DR. *M. tuberculosis* strains lacking surface lipid phthiocerol dimycocerosate are susceptible to killing by an early innate host response. Infect Immun 2014;82:5214–22.

[40] Muñoz-Elías EJ, McKinney JD. *Mycobacterium tuberculosis* isocitrate lyase 1 and 2 are jointly required for in vitro growth and virulence. Nat Med 2005;11:735–8.

[41] Huard RC, Chitale S, Leung M, Lazzarini LCO, Zhu H, Shashkina E, Laal S, Conde MB, Kritski AL, Belisle JT, Kreiswirth BN, Lapa e Silva JR, Ho JL. The *M. tuberculosis* complex-restricted gene *cfp32* encodes an expressed protein that is detectable in tuberculosis patients and is positively correlated with pulmonary interleukin-10. Infect Immun 2003;71:6871–83.

[42] Fenhalls G, Stevens L, Moses L, Bezuidenhout J, Betts JC, Helden Pv Pv, Lukey PT, Duncan K. In situ detection of *M. tuberculosis* transcripts in human lung granulomas reveals differential gene expression in necrotic lesions. Infect Immun 2002;70:6330–8.

[43] Xu WX, Zhang L, Mai JT, Peng RC, Yang EZ, Peng C, Wang HH. The Wag31 protein interacts with AccA3 and coordinates cell wall lipid permeability and lipophilic drug resistance in *Mycobacterium smegmatis*. Biochem Biophys Res Commun 2014;448:255–60.

[44] Florczyk MA, Mccue LA, Stack RF, Hauer CR, Mcdonough KA. Identification and characterization of mycobacterial proteins differentially expressed under standing and shaking culture conditions, including Rv2623 from a novel class of putative ATP-Binding proteins. Infect Immun 2001;69:5777–85.

[45] Drumm JE, Mi K, Bilder P, Sun M, Lim J, Bielefeldt-Ohmann H, Basaraba R, So M, Zhu G, Tufariello JM, Izzo AA, Orme IM, Almo SC, Leyh TS, Chan J. *Mycobacterium tuberculosis* universal stress protein Rv2623 regulates bacillary growth by ATP-binding:requirement for establishing chronic persistent infection. PLoS Pathog 2009;5:e1000460.

[46] Singh SK, Singh SK. The *Mycobacterium tuberculosis* H37Ra gene MRA_1916 causes growth defects upon down-regulation. Sci Rep 2015;5:16131. https://doi.org/10.1038/srep16131.